Biomaterials 64 (2015) 115–124

Contents lists available at ScienceDirect

Biomaterials

journal homepage: www.elsevier.com/locate/biomaterials

Self-assembling bubble carriers for oral protein delivery

Er-Yuan Chuang [a, 1], Kun-Ju Lin [b, c, 1], Po-Yen Lin [a, 1], Hsin-Lung Chen [a], Shiaw-Pyng Wey [b], Fwu-Long Mi [d], Hsu-Chan Hsiao [a], Chiung-Tong Chen [e, **], Hsing-Wen Sung [a, *]

[a] Department of Chemical Engineering and Institute of Biomedical Engineering, National Tsing Hua University, Hsinchu, Taiwan, ROC
[b] Department of Medical Imaging and Radiological Sciences, College of Medicine, Chang Gung University, Taoyuan, Taiwan, ROC
[c] Department of Nuclear Medicine and Molecular Imaging Center, Chang Gung Memorial Hospital, Taoyuan, Taiwan, ROC
[d] Department of Biochemistry and Molecular Cell Biology, College of Medicine, Taipei Medical University, Taipei, Taiwan, ROC
[e] Institute of Biotechnology and Pharmaceutical Research, National Health Research Institutes, Zhunan, Miaoli, Taiwan, ROC

ARTICLE INFO

Article history:
Received 14 April 2015
Received in revised form
11 June 2015
Accepted 18 June 2015
Available online 20 June 2015

Keywords:
Foaming agent
Colloidal carrier
Oral protein delivery
Surfactant
Biodistribution

ABSTRACT

Successful oral delivery of therapeutic proteins such as insulin can greatly improve the quality of life of patients. This study develops a bubble carrier system by loading diethylene triamine pentaacetic acid (DTPA) dianhydride, a foaming agent (sodium bicarbonate; SBC), a surfactant (sodium dodecyl sulfate; SDS), and a protein drug (insulin) in an enteric-coated gelatin capsule. Following oral administration to diabetic rats, the intestinal fluid that has passed through the gelatin capsule saturates the mixture; concomitantly, DTPA dianhydride produces an acidic environment, while SBC decomposes to form CO_2 bubbles at acidic pH. The gas bubbles grow among the surfactant molecules (SDS) owing to the expansion of the generated CO_2. The walls of the CO_2 bubbles consist of a self-assembled film of water that is in nanoscale and may serve as a colloidal carrier to transport insulin and DTPA. The grown gas bubbles continue to expand until they bump into the wall and burst, releasing their transported insulin, DTPA, and SDS into the mucosal layer. The released DTPA and SDS function as protease inhibitors to protect the insulin molecules as well as absorption enhancers to augment their epithelial permeability and eventual absorption into systemic circulation, exerting their hypoglycemic effects.

1. Introduction

Oral delivery of therapeutic proteins such as insulin can avoid the pain and discomfort associated with injections and greatly improve the quality of life of patients. Nevertheless, oral absorption of insulin is limited by hostile gastric and intestinal environments and by the poor epithelial permeability [1]. Experiments have shown that enteric-coated gelatin capsules containing insulin with protease inhibitors and absorption enhancers orally administered to rats can achieve increased plasma insulin levels and corresponding reductions in blood glucose [2]. The enteric coating is a pH-responsive polymer barrier, so the capsule remains intact in the highly acidic pH environment of the stomach; conversely, as the body fluid from the intestinal tract (neutral or slightly basic pH) comes into contact with the enteric-coated capsule, the water soluble polymer and gelatin dissolve and the drug load diffuses through the resulting pores.

However, the enteric polymer coated on the gelatin capsule does not dissolve instantly or completely in the small intestine because of its partial contact with the body fluid. Thus, a certain amount of the encapsulated protein drugs within the capsule might remain stuck within the partially dissolved capsule (Fig. 1). Another problem is that protein molecules may aggregate during their exposure to body fluid, which can limit their interaction with and entrance into epithelial cells and reduce their oral bioavailability. Therefore, increasing the bioavailability of oral protein drugs to a therapeutically acceptable level is still challenging.

To provide quick and effective delivery of a drug load from enteric-coated gelatin capsules, this study develops a novel carrier system that involves a foaming agent (sodium bicarbonate; SBC) that can generate CO_2 bubbles upon exposure to an acidic aqueous environment. The walls of these CO_2 bubbles consist of a nanoscale self-assembled film of water that can be sandwiched between two

* Corresponding author. Department of Chemical Engineering, National Tsing Hua University, Hsinchu, 30013, Taiwan, ROC.
** Corresponding author.
E-mail addresses: ctchen@nhri.org.tw (C.-T. Chen), hwsung@mx.nthu.edu.tw (H.-W. Sung).
[1] The first three authors contributed equally.

http://dx.doi.org/10.1016/j.biomaterials.2015.06.035
0142-9612/

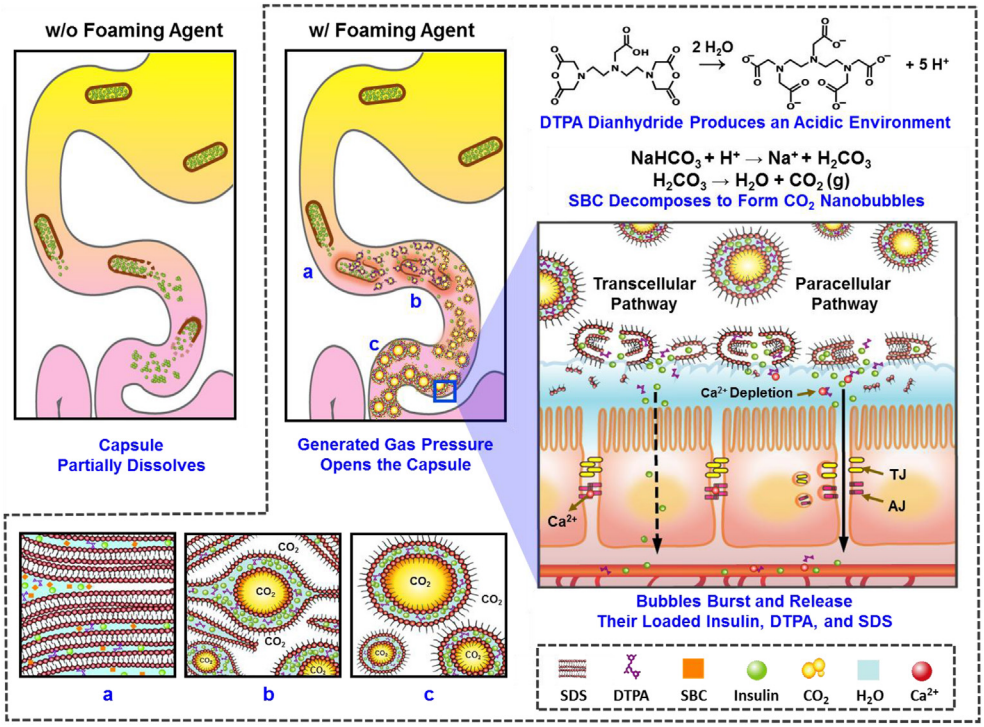

Fig. 1. Schematic illustrations showing the formation and expansion of bubble carriers (see subfigures a, b, and c) developed from the orally administered gelatin capsule and their mechanism for delivering insulin across the epithelial barrier. TJ: tight junction; AJ: adherens junction.

layers of surfactant molecules to form a colloidal carrier for transporting protein drugs. Absorption can be increased by formulating the drug as a solubilizate within a colloidal dispersion [3]. This bubble carrier system is prepared by mixing diethylene triamine pentaacetic acid (DTPA) dianhydride, SBC, a surfactant (sodium dodecyl sulfate; SDS), and a protein drug (insulin). The DTPA dianhydride is an acidic oxide that dissolves in water to form an acid (DTPA) solution [4]. When reacting with the acid, SBC produces a bubbly CO_2 gas [5].

Fig. 1 shows a schematic of this bubble carrier system and how it works. When the water that passes through the gelatin capsule saturates the mixture, nanosized CO_2 bubbles are generated. As the gas pressure opens the capsule, the load is quickly released. The gas bubbles grow among the surfactant molecules, expanded by the generated CO_2. The reaction also proceeds outside the formed bubbles, which are therefore effectively suspended in a gas-rich environment. The SDS is an anionic surfactant consisting of a hydrophilic (water-loving) head and a hydrophobic (water-hating) tail. As the gas bubbles expand, the hydrophobic tail of each surfactant molecule is attracted to the gas-rich phase while their hydrophilic head is attracted to the water phase. Therefore, a bubble carrier system comprising a water film containing insulin and DTPA is self-assembled between double layers of surfactant molecules (SDS). The gas bubbles continue to expand until they come in contact with the mucosal layer covering the intestinal wall and eventually burst and release their loads of insulin, DTPA, and SDS. In the mucosal layer, DTPA serves a paracellular enhancer for delivering insulin molecules through the epithelial cells, and the amphiphilic surfactant (SDS) enhances their paracellular and transcellular permeability. Both DTPA and SDS also protect insulin molecules by functioning as protease inhibitors [2,6].

We hypothesize that the proposed bubble carrier system can mediate temporary alterations in the morphology of epithelial cell membranes and transient opening of their apical junctional complexes (AJCs), which facilitates the encapsulated insulin molecules in crossing the epithelial barrier and eventually being absorbed into systemic circulation, where they exert hypoglycemic effects.

2. Materials and methods

2.1. Materials

The SBC, DTPA dianhydride, SDS, and insulin (from bovine pancreas, 27.4 IU/mg) were obtained from Sigma–Aldrich (St. Louis, MO, USA). The fluorescein isothiocyanate (FITC)-insulin (bovine) and cyanine 3 (Cy3) were purchased from Invitrogen Corp. (Carlsbad, CA, USA) and Lumiprobe Corp. (Broward, FL, USA), respectively, and ^{123}I was acquired from Institute of Nuclear Energy Research (Taoyuan, Taiwan). All other chemicals and reagents used were of analytical grade.

2.2. Preparation of test capsules

Hard gelatin capsules (size 9; Torpac Inc., Fairfield, NJ, USA) were manually filled with a mixture of SBC (8.0 mg), DTPA dianhydride (8.0 mg), SDS (4.0 mg), and insulin (0.38 mg) according to manufacturer instructions. The capsules without SBC were used as a control. The prepared capsules were immersed in a methanol solution of Eudragit® L100-55 (15% w/v, Evonik Industries, Parsippany, NJ, USA) and then dried at room temperature using an air-blower; this procedure was repeated three times.

2.3. Characterization of test capsules

The *in vitro* dissolution of test capsules was performed in test tubes containing a phosphate buffered saline (PBS) solution at pH 2.0, pH 6.6, or pH 7.4 (adjusted by HCl); the test tubes were

immersed in a water-filled tank at 37 °C. An ultrasound imaging system with a 7 MHz linear-array transducer (Z-one, Zonare, Mountain View, CA, USA) was used to visualize the generated CO_2 bubbles; consecutive ultrasonic B-mode images were recorded with a computer.

2.4. Structural analysis of bubble carriers

The formation of bubble carriers and their structural changes as the gas bubbles expanded were examined by fluorescence microscopy (Axio Observer; Carl Zeiss, Jena, Germany), transmission electron microscopy (TEM; JEOL 2010F, Tokyo, Japan), and small angle X-ray scattering (SAXS). For the TEM observation, a drop of sample solution immediately after reaction was placed on the copper grid, and blot-dried using a filter paper, followed by dropping 1% osmium tetroxide (OsO_4), a preferential staining agent for the double bonds of unsaturated compounds (*e.g.*, SDS) [7], solution onto the grid and blot-dried again.

For the SAXS experiments, test samples were injected into sample cells composed of two Kapton windows [8]. The measurements were performed using the BL23A1 beamline at the National Synchrotron Radiation Research Center (NSRRC), Hsinchu, Taiwan. The energy of the beam source was 15.0 keV, and the sample-to-detector distance was 3060.3 mm. The scattering intensity profile was obtained after corrections for sample transmission, empty cell transmission, empty cell scattering, and the sensitivity of the detector. Scattering intensity I(Q) was plotted as a function of scattering vector, $Q=(4\pi/\lambda)\sin(\theta/2)$ (θ = scattering angle). The resolvable time scale for this instrument is under 10 s. A two-dimensional Pilatus 1 M detector with 981 × 1043 pixel resolution was used to record the SAXS profiles.

2.5. Investigation of the mechanism of epithelial permeability

The Caco-2 cell monolayers were grown on a tissue-culture-treated polycarbonate filter in a Costar Transwell with twelve wells/plate (Corning Costar Corp., NY, USA) and then treated with test samples (DTPA or SDS, 2.0 mg/mL, 1.0 mL) containing FITC-insulin for 2 h; translocation of their AJC proteins was then analyzed by immunofluorescence staining. After washing the cells three times with pre-warmed PBS, the cells were fixed and permeabilized in 100% acetone for 10 min at −20 °C. Non-specific binding was blocked in 5% normal goat serum (Jackson ImmunoResearch Laboratories, West Grove, PA, USA) in PBS for 60 min at 37 °C. The cells were then incubated overnight in primary antibodies [mouse anti-claudin-4 (Invitrogen) and donkey anti-E-cadherin (Abcam, Cambridge, MA, USA)] at 4 °C. Results were visualized by applying appropriate Alexa-Fluor-conjugated secondary antibodies (Invitrogen); the cells were also counterstained with DAPI (Invitrogen) for examination by inverted confocal laser scanning microscopy (CLSM; Zeiss LSM780, Carl Zeiss, Jena GmbH, Germany).

Extracellular calcium levels were detected by staining the treated cells with 40.0 mM Alizarin Red S (ARS; Sigma–Aldrich), pH 4.0, for 10 min followed by washing with 70% ethanol and with PBS to remove non-specific staining. Samples were then visualized by an inverted phase-contrast light microscope (Nikon Eclipse-Ti, Nikon Instruments Inc., Melville, NY, USA).

2.6. Evaluation of inhibition of proteolytic degradation

In vitro inhibition of intestinal proteases by DTPA and SDS was separately studied in the proximal portion of the small intestine freshly isolated from rats (Wistar). The intestinal tissues were incubated with a Krebs–Ringer buffer containing insulin (1.0 mg/mL, 1.0 mL) and DTPA or SDS (2.0 mg/mL, 1.0 mL) at 37 °C. The remaining amount of intact insulin was quantified by high-performance liquid chromatography (HPLC) analysis of test solutions (50.0 μL) withdrawn at different time intervals, based on a protocol described in the literature [9].

2.7. Animal study

All animal studies were performed according to the "Guide for the Care and Use of Laboratory Animals", which was prepared by Institute of Laboratory Animal Resources, National Research Council, and published by the National Academy Press in 1996. All studies were also approved by the Institutional Animal Care and Use Committee of National Tsing Hua University (protocol number 10046).

2.8. In vivo dissolution of test capsules and biodistribution of insulin

Insulin was radiolabeled with Iodine-123 (^{123}I) using an iodogen-tube (Pierce Iodination Tubes, Thermo Fisher Scientific, Rockford, IL, USA) according to a method reported in the literature [10]; previous radiochemical stability tests in human serum showed that 91% of the isotope-labeled compound remained intact after incubation for 24 h. After purification, the obtained ^{123}I-insulin was lyophilized for further studies. The dynamic plain X-ray and scintigraphy images of rats (Wistar, *ca.* 250 g, n = 3) were acquired at predetermined time intervals after oral administration of test capsules containing ^{123}I-insulin and barium sulfate, a radiocontrast agent.

The biodistribution of insulin in the intestinal tract was investigated by *in vivo* imaging system (IVIS). At predetermined time points after oral ingestion of test capsules containing FITC-insulin, the rats (n = 3) were sacrificed. The gastrointestinal (GI) tracts were then harvested, irradiated (FITC excitation wavelength, 495 nm), and imaged with an appropriate emission filter (519 nm) to obtain FITC images. The retrieved tissues were also washed three times with PBS, fixed in 3.7% paraformaldehyde, processed for cryosectioning, and then examined under CLSM.

The biodistribution of insulin absorbed into systemic circulation was examined by a single-photon emission computed tomography (SPECT)/computed tomography (CT) scanner (n = 3 rats). After the last SPECT scan, additional whole-body CT images of the internal organs were acquired after intravenous administration of the Conray™ contrast agent (Mallinckrodt, MO, USA). The amount of contrast fluid stasis in the vasculature was maximized by slowly injecting the contrast agent *via* the tail vein (2.0 mL over 40 s). After receiving half of the Conray™ dose, each animal was sacrificed by co-injection of potassium chloride under deep anesthesia. The image scanning was performed using the protocol described in a previous work by this research group [11].

2.9. In vivo toxicity

The toxicity of the test capsule was evaluated in rats, which were randomly divided into two groups. For 14 days, the experimental group orally received daily a dose of the capsules that contained DTPA dianhydride, SDS and SBC (100 mg/kg, n = 6 for each gender), while the other untreated group was a control. Animals were observed carefully for the onset of any signs of toxicity and monitored for changes in body weight. After the animals had been sacrificed, internal organs of each animal were harvested and observed grossly. For sectional histology, intestine, liver and kidney specimens were fixed in 10% phosphate buffered formalin, embedded in paraffin, cross-sectioned at 5 μm and then stained

with hematoxylin and eosin (H&E).

2.10. Examination of the pharmacokinetic (PK) and pharmacodynamic (PD) profiles

Diabetes was induced in rats *via* intraperitoneal injection of streptozotocin as described previously [12]. The rats were then fasted overnight and for the remainder of the experiment but with free access to the water. The following formulations were administered individually to the diabetic rats: an enteric-coated capsule containing free-form insulin powder alone (30.0 IU/kg, oral); an enteric-coated capsule filled with DTPA dianhydride, SDS, insulin (30.0 IU/kg), together with or without SBC (oral); and a subcutaneous (SC) injection of free-form insulin solution (5.0 IU/kg) ($n = 6$ for each studied group). Blood samples were taken from the tail veins before administering the drug and at varying time intervals after dosing. The blood glucose levels were then measured with a glucose meter (LifeScan, Milpitas, CA, USA). Plasma insulin levels were determined by centrifuging blood samples (10,000 rpm, 4 °C, for 15 min) with subsequent quantification using ELISA (bovine insulin kit, Mercodia AB, Uppsala, Sweden). The formula used to calculate the relative bioavailability (BA_R) of insulin after the treatments was

$$BA_R = \frac{AUC_{(oral)} \times Dose_{(SC)}}{AUC_{(SC)} \times Dose_{(oral)}} \times 100\%$$

where AUC represents the total area under the plasma insulin concentration *vs.* time curve.

2.11. Statistical analysis

Average data were reported as means ± SD. Statistical analyses were performed with SPSS (Chicago, IL, USA). One-tailed Student *t* test was used for statistical comparisons of the two groups. A *P* value less than 0.05 was considered statistically significant.

3. Results and discussion

This study evaluated the feasibility of using the proposed bubble carrier system for oral insulin delivery. The DTPA dianhydride, SBC (foaming agent), SDS, and insulin were thoroughly mixed and loaded in hard gelatin capsules. The capsules were then coated with an enteric polymer (Eudragit® L100-55), which is dissoluble above pH 5.5 for protecting the loaded contents from gastric fluid [13,14]. The control was enteric-coated capsules without SBC.

3.1. In vitro dissolution of test capsules

The dissolution of the enteric-coated capsules with or without SBC was evaluated *in vitro* in conditions simulating the pH environments in the GI tract. In this experiment, trypan blue was included in the test capsules as a dye indicator. The generation of CO_2 bubbles was investigated using an ultrasound machine. According to Fig. 2a, both test capsules remained intact at pH 2.0 (mimicking the acidic milieu in the stomach) [15], confirming the gastroresistant feature of Eudragit® L100-55. In the pH environments of the small intestine (pH 6.6 and pH 7.4) [16], the load diffused through the pore that developed as the enteric polymer coated on the control capsule (containing no SBC) slowly dissolved. The absence of ultrasound signals in this case suggests that no bubbles were generated.

Conversely, following partial dissolution of the enteric polymer and penetration of water into the gelatin capsule containing DTPA dianhydride and SBC, gas bubbles were immediately produced (Fig. 2b). When DTPA dianhydride is exposed to water, an acidic environment is produced [17], in which SBC decomposes to form CO_2 bubbles that are hyperechogenic and could act as a contrast enhancer for ultrasound imaging [18]. The resulting gas pressure forced the capsule to open and quickly released its loaded contents.

3.2. Formation of bubble carriers

To identify their locations within the generated gas bubbles, insulin was labeled with a green fluorescence dye (FITC) while DTPA was marked with a red fluorescence dye (Cy3); the test samples were then viewed under a fluorescence microscope. Structural changes caused by expansion of the gas bubbles were observed by TEM and by SAXS. Fig. 3a shows that the insulin molecules released from the capsule without SBC tended to aggregate upon exposure to water. A well-known effect of water sorption by protein molecules is the production of structural transitions that cause aggregation and other deleterious phenomena [19].

Conversely, as the contents of the capsule with the foaming agent were released and exposed to water, CO_2 bubbles in nanoscale were self-assembled (Fig. 3b). The obtained TEM and fluorescence micrographs demonstrate that the gas bubbles grew from nanoscale (Fig. 3b) to microscale (Fig. 3c and d) among the surfactant molecules (SDS) owing to the expansion of the generated CO_2. The gas bubbles were surrounded by a layer (thickness, approximately 150 nm) of green (Fig. 3c) and red (Fig. 3d) fluorescence indicating insulin and DTPA molecules, respectively. As the gas bubbles expanded, the hydrophilic heads of SDS remained solvated in the water phase, and the hydrophobic tails were extended into the gas-rich environment which is generally considered hydrophobic [20], as schematically illustrated in Fig. 3e. Thus, a self-assembled film of water sandwiched between the two layers of surfactant molecules stabilized the generated gas bubbles; the self-assembled water film could also serve as a colloidal carrier to encapsulate the hydrophilic insulin and DTPA molecules. The locations of insulin and DTPA after bubble formation are important for their subsequent delivery.

Fig. 3f shows the results of time-resolved SAXS performed to reveal the structural changes in gas bubbles during their formation. When the SDS in powder form came in contact with water ($t = 0$ s, first row in Fig. 3c–e), the SAXS profile showed two sharp peaks corresponding to (001) and (002) diffractions of a multilamellar structure, signifying that the surfactant molecules in the powder had self-assembled into a multilamellar structure with an interlamellar distance of *ca.* 4.0 nm. At 30 s after reaction, the original primary peak transformed into a broad halo and the second-order peak vanished. This result indicates that the multilamellar structure was disrupted by the generated CO_2 bubbles to yield oligolamellar carriers composed of gas bubbles surrounded by water films (second row in Fig. 3c–e). The progressive diminishment of the primary peak in the SAXS profiles suggested that the number of layers of surfactant molecules decreased as the reaction proceeded. After 240 s, the SAXS peaks were no longer visible, which indicated the formation of unilamellar carriers (third row, Fig. 3c–e).

3.3. Enhanced epithelial permeability

Drug permeation may occur across the intestinal epithelium and through either transcellular or paracellular routes [21]. To elucidate the precise mechanisms of interactions between the bubble carrier system and epithelial cells and its subsequent transport of the drug, the effects of DTPA and SDS on epithelial permeability were individually studied using Caco-2 cell monolayers. Monolayers of Caco-

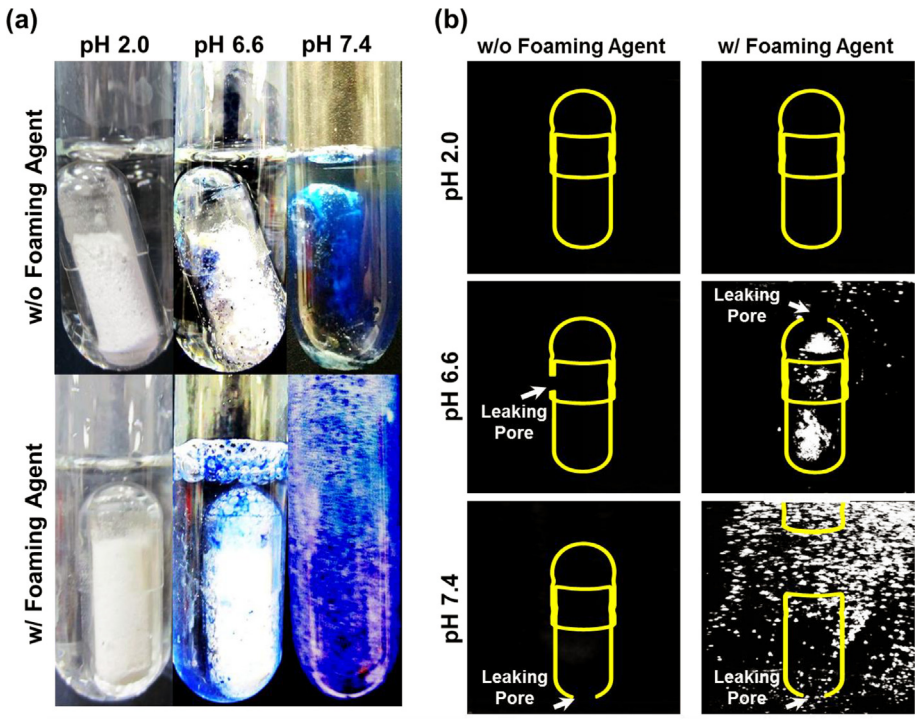

Fig. 2. (a) Results of the dissolution and disintegration of test capsules with or without SBC evaluated *in vitro* under varying pH to simulate the pH environments in the GI tract; (b) ultrasound images showing the generation of CO_2 bubbles.

2 cells derived from human colorectal adenocarcinoma are widely used in *in vitro* models for predicting intestinal drug permeability [22].

The AJC, which is comprised of adherens junctions (AJs) and tight junctions (TJs), is an important regulator of the intestinal cell structure and the epithelial barrier function. The AJs cause plasma membranes to combine, and they enhance TJ assembly; alteration of AJs therefore modulates the TJ structure and epithelial permeability [12]. Claudin-4 (CLDN4) is a TJ protein whereas E-cadherin [23], a calcium (Ca^{2+})-dependent adhesion molecule, is the major transmembrane protein of AJs. Accordingly, extracellular Ca^{2+} is essential for formation of AJC and maintenance of cell–cell junctions [24]. Both AJs and TJs can rapidly disassemble and reorganize in response to various extracellular stimuli [25].

Fig. 4 shows the extracellular Ca^{2+} levels (as indicated by the ARS-labeled Ca^{2+}) and the immunofluorescence staining of Caco-2 cell monolayers before and after exposure to FITC-insulin combined with either DTPA or SDS. Following treatment with test samples, the ultrastructural changes in Caco-2 cell monolayers were directly visualized by CLSM. The DTPA treatment significantly reduced extracellular calcium levels; additionally, both CLDN4 and E-cadherin clearly revealed intracellular internalization. Since DTPA is a well-known complexing agent that chelates divalent metal ions such as Ca^{2+} [2], it disrupted the epithelial AJCs and thereby enhanced the permeability of insulin *via* the paracellular pathway.

Conversely, SDS treatment caused insulin molecules to permeate Caco-2 cells *via* both the paracellular and transcellular routes. Previous studies reported that SDS enhances protein drug absorption across the intestinal epithelium [26]. The increased paracellular permeability caused by SDS might result from transient depletion of cellular ATP whereas enhanced transcellular absorption is associated with an altered cell morphology [27]; however, this alteration is reversible [28].

3.4. Inhibition of proteolytic degradation

Inhibiting the proteolytic degradation of insulin in the intestinal fluid and the mucosal layer is critical for increasing its oral bioavailability. The inhibiting effects of DTPA and SDS on intestinal proteases were separately studied in *in vitro* studies of the proximal portion of the small intestine (*i.e.*, the duodenum) freshly isolated from rats. The various digestive enzymes secreted from the pancreas into the duodenum are well-recognized [29]. The HPLC was used to quantify the remaining amount of intact insulin. According to Fig. 5, free-form insulin molecules were rapidly degraded by the proteolytic enzymes that were present in the mucosal layer that covered the intestinal wall; however, the addition of DTPA or SDS in insulin produced a strong protective effect against the intestinal proteases ($P < 0.05$). Insulin is highly sensitive to trypsin and chymotrypsin, which are Ca^{2+}-dependent enzymes in the intestinal fluid and in the mucosal layer [30]. One strategy for inhibiting intestinal protease activities is using complexing agents such as DTPA to remove essential metal ions (*e.g.*, Ca^{2+}) from the enzyme structure. A previous study indicated that SDS has a binding affinity for both free enzymes and the enzyme-substrate binary complex. Proposed molecular mechanisms of proteolytic inhibition by SDS include local conformational changes or altered charge distributions of the proteases induced by their specific binding of SDS [31].

3.5. In vivo dissolution of the test capsule and its subsequent release of insulin

In the *in vivo* dissolution study, the capsule with SBC was orally administered to rats using a gavage needle; its counterpart containing no SBC served as a control. In this experiment, insulin was radiolabeled with ^{123}I; additionally, a radiocontrast agent, barium sulfate, was incorporated in the test capsules. A SPECT/CT scanner

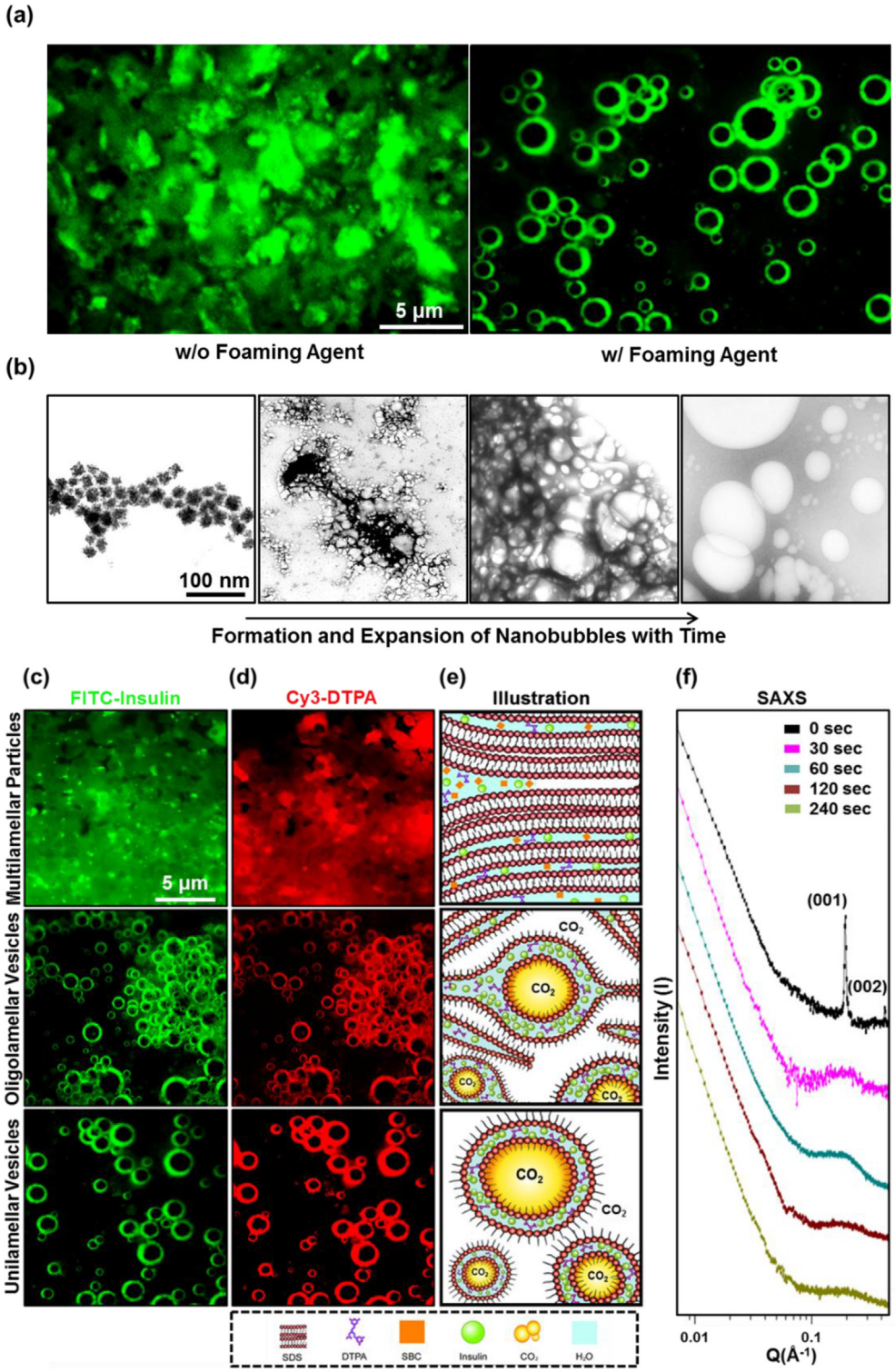

Fig. 3. (a) Fluorescence images showing the dispersion of the FITC-labeled insulin released from the capsule with or without the foaming agent (SBC) upon exposure to water; (b) TEM micrographs showing the evolution and expansion of nanobubbles generated by the capsule containing SBC. Fluorescence images revealing encapsulation of both (c) FITC-insulin and (d) Cy3-DTPA within the water film of the bubble carriers; (e) corresponding schematic illustrations displaying the bubble carriers produced upon exposure to water; (f) SAXS profiles showing structural changes in the formation and expansion of bubble carriers.

was used for imaging. The dynamic plain X-ray and scintigraphy images of the rats were acquired sequentially at 2 min intervals for 1 h after oral administration of the test capsules. Fig. 6a shows that, once the capsule left the stomach, the CO_2 generated in the pH environment of the small intestine immediately disintegrated the SBC capsule; the ^{123}I-labeled insulin was then rapidly released (white arrow). During this time, the capsule without the foaming agent remained intact.

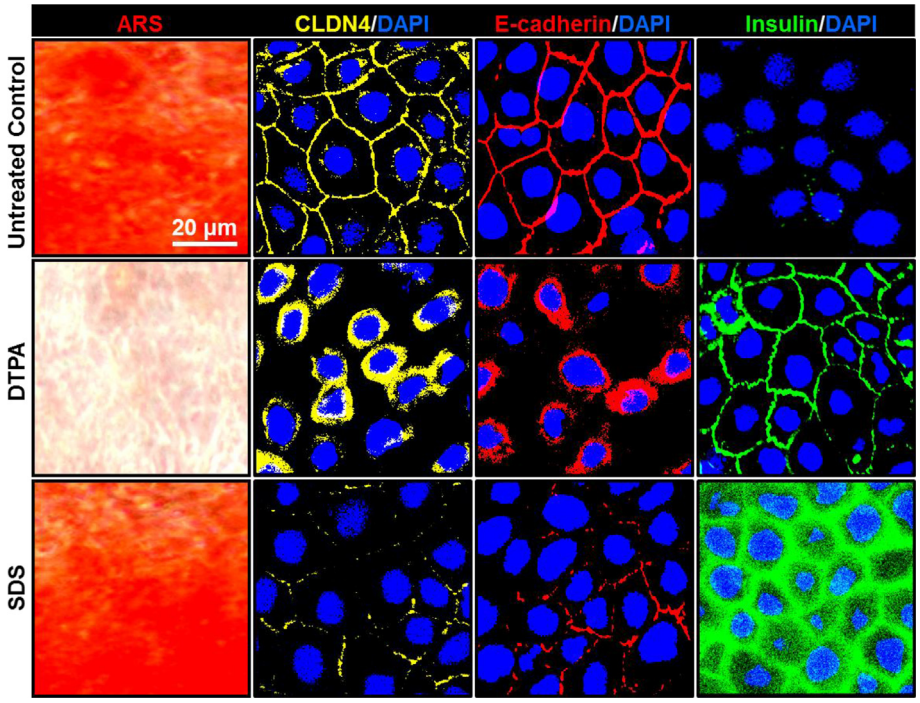

Fig. 4. Photomicrographs showing the extracellular calcium levels (red ARS-labeled Ca^{2+}) and immunofluorescence staining results for Caco-2 cell monolayers treated with DTPA or SDS in the presence of FITC-insulin. (For interpretation of the references to color in this figure legend, the reader is referred to the web version of this article.)

3.6. Intestinal biodistribution and absorption of the released insulin

Next, FITC-labeled insulin was used to visualize the biodistribution of the insulin released from test capsules in the intestinal tract and its subsequent absorption into the villi. At predetermined time points after oral ingestion of the test capsules, the rats were sacrificed, and their GI organs were retrieved and examined with an IVIS. Cryosections of the retrieved intestinal villi were also inspected with a CLSM. Fig. 6b shows that the FITC-insulin was released into the intestinal tract more rapidly and at higher concentrations in the group that received the capsule with SBC compared to the group that received the capsule without SBC. In the former case, the difference most likely resulted from formation of gas bubbles which generated forces that increased dispersion of the released insulin molecules and avoided their aggregation. After oral ingestion, dispersion of the drug molecules in the intestinal milieu is a prerequisite for their absorption [32].

The bubble carriers formed with a water film containing insulin and DTPA sandwiched between two layers of SDS (Fig. 3). They then drifted in the intestinal lumen until they eventually bumped into the intestinal wall and burst, releasing their loaded insulin, DTPA, and SDS into the mucosal layer (Fig. 1). The released insulin, DTPA, and SDS then infiltrated the mucosal layer and accessed the epithelium surface. The presence of green fluorescence (FITC-insulin) on the lacteal side of the villi demonstrate that DTPA and SDS protect insulin molecules from proteolytic degradation and enhance their epithelial permeability and absorption into systemic circulation (Fig. 6c). Notably, the green fluorescence intensity was higher in the group treated with the SBC capsule compared to the group treated with the control capsule containing no SBC, indicating that the developed bubble carrier system is a promising vehicle for orally administered insulin.

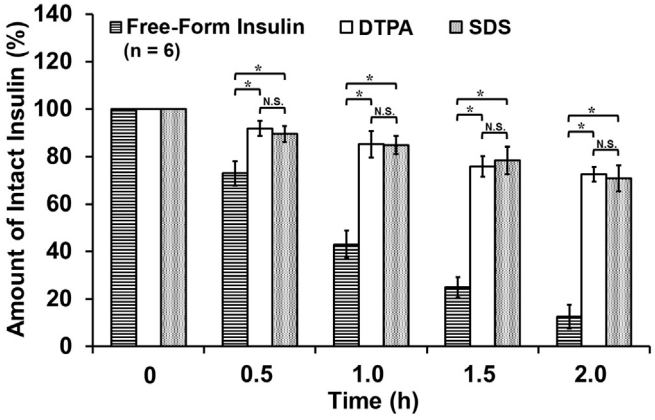

Fig. 5. Results of insulin degradation in the presence or absence of DTPA or SDS in proximal intestinal segments freshly isolated from rats. N.S.: not significant; *: statistically significant ($P < 0.05$).

3.7. Systemic biodistribution of the absorbed insulin

The systemic biodistribution of the absorbed ^{123}I-insulin was investigated by SPECT/CT over a 4-h period after ingestion of the test capsules. The radioactivity of ^{123}I-insulin was presented in rainbow pseudo-color scale and superimposed on the CT images (gray color) to distinguish anatomic localizations. In both groups, the accumulation of radioactivity in the heart, kidney, and urinary bladder indicated systemic absorption of ^{123}I-insulin (Fig. 6d). The rapid release of the drug load as the test capsule was disintegrated by the bubble pressure produced a high local concentration of the drug. Since transport to the blood is a function of the local drug concentration, rapid release of a high concentration results in rapid transport of the drug. Therefore, the radioactivity of ^{123}I-insulin in systemic circulation was earlier and stronger in the group that received the SBC test capsule compared to the control group that received the capsule without SBC.

For a further illustration of the enhanced uptake of insulin in systemic circulation conferred by the bubble carriers in the group

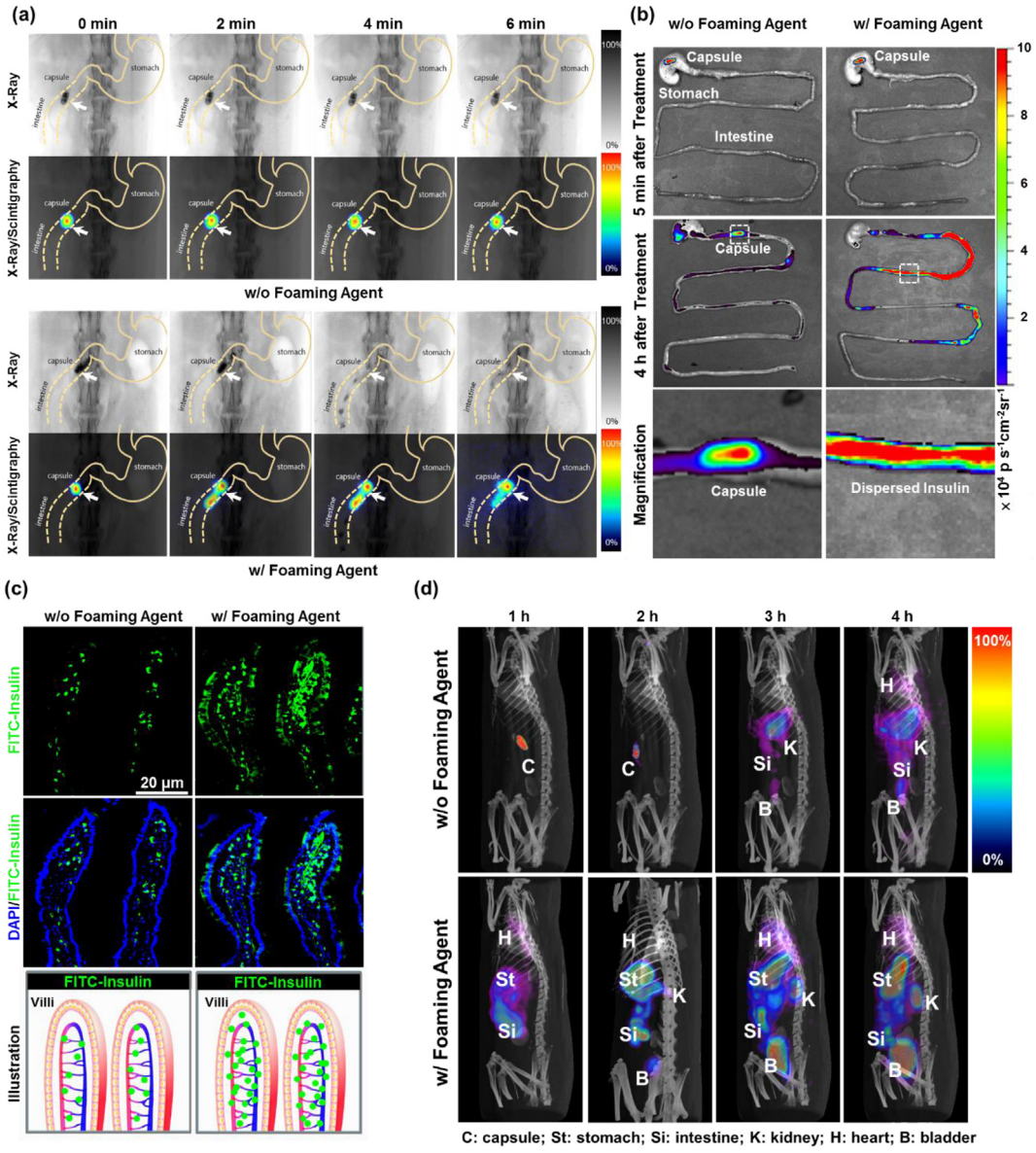

Fig. 6. (a) Sequential plain X-ray and X-ray/scintigraphy images of test rats orally treated with the capsules containing barium sulfate and ^{123}I-isulin (white arrow) with or without foaming agent. (b) The IVIS fluorescent images of FITC-insulin released from capsules with or without foaming agent during their transit in the GI tract; (c) CLSM images of frozen intestinal sections with schematic diagram of insulin absorption into the villi. (d) Biodistribution of ^{123}I-insulin illustrated by contrast-enhanced tomographic images. The intensities of ^{123}I-insulin in different organs are shown in rainbow pseudo-color scale.

that orally received the capsule containing SBC, the Supplementary Information provides a time-lapse 3D video; the group orally treated with the capsule without SBC was used as a control. The video shows that, after ingestion, the test capsule with SBC disintegrated faster and more completely compared to the control capsule without the foaming agent, producing a higher local concentration of the released insulin. Thus, absorption of insulin into systemic circulation in the case incorporating the foaming agent was much quicker and more pronounced than in the case containing no foaming agent.

Supplementary video related to this article can be found at http://dx.doi.org/10.1016/j.biomaterials.2015.06.035.

3.8. *In vivo* toxicity

In the *in vivo* toxicity investigation, for 14 days, rats were treated daily with a dose of the capsules that contained SBC; untreated rats formed a control group. According to Fig. S1a, the body weights of the rats in the experimental group (male and female) increased slightly over time in a manner similar to those of the untreated control group ($P > 0.05$). The reduction in body-weight is commonly regarded a simple and sensitive index of *in vivo* toxicity [11]. No apparent tissue damage or toxic effects in organs (small intestine, liver and kidney) were observed (Fig. S1b). Generally, a specific tissue-level toxicological study is concerned with inflammation (intestine), hepatotoxicity (liver), and nephrotoxicity (kidney) responses [11]. The analytical results herein suggest no significant *in vivo* toxicity following treatment with the SBC capsule.

3.9. *In vivo* PK and PD profiles

The PK and PD profiles of the diabetic rats that received the capsules with or without SBC were also analyzed. The control

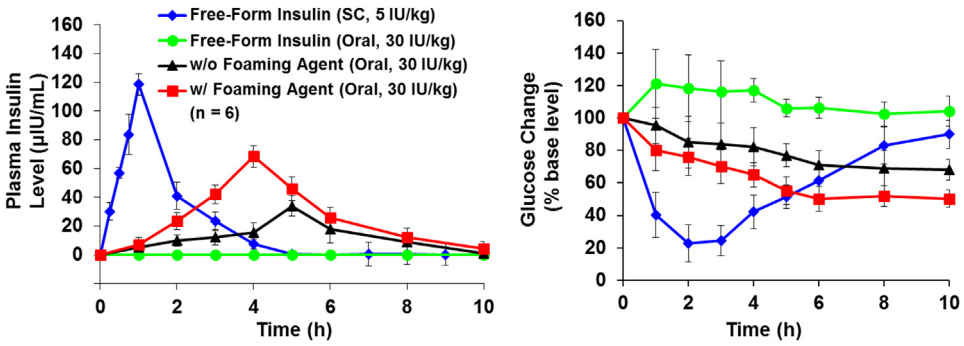

Fig. 7. Plasma insulin level *vs.* time profiles and blood glucose change *vs.* time profiles of diabetic rats treated with varying insulin formulations. Oral: oral administration of test capsules and SC: subcutaneous injection.

Table 1
The PK parameters of insulin in diabetic rats given varying insulin formulations (n = 6).

	Free-form insulin (SC)[a]	Free-form insulin (Oral)[b]	w/o foaming agent (Oral)[b]	w/ Foaming agent (Oral)[b]
Dose [IU/kg]	5.0	30.0	30.0	30.0
C_{max}[c] [μIU/mL]	119.6 ± 3.8	1.8 ± 0.7	34.0 ± 6.4	68.4 ± 6.8
T_{max}[d] [h]	1.0	5.0	5.0	4.0
$AUC_{(0-10\ h)}$[e] [μIU h/mL]	191.3 ± 30.7	6.5 ± 2.7	123.8 ± 28.4	249.2 ± 34.1
BA_R[f] [%]	100	0.5 ± 0.3	10.8 ± 3.1	21.7 ± 1.7

[a] Subcutaneous injection.
[b] Oral administration of test capsules.
[c] Maximum plasma concentration.
[d] Time at which C_{max} is attained.
[e] Area under the plasma concentration-time curve.
[f] Relative bioavailability of insulin.

groups received free-form insulin solution *via* SC injection or the capsule containing the free-form insulin powder alone *via* oral ingestion. Fig. 7 shows that SC injection of free-form insulin solution resulted in a maximum plasma concentration at 1 h post administration, which caused a sharp decrease in the blood glucose level within 1–3 h before returning to its basal level. As expected, oral administration of the capsule filled with the free-form insulin powder produced no hypoglycemic effects, indicating the poor oral absorption of insulin in the absence of a suitable delivery system.

Conversely, measurable concentrations of insulin were obtained within an hour of administration of the capsules containing protease inhibitors/absorption enhancers (DTPA and SDS), producing a steady plasma concentration of drug for over 10 h with maximum insulin concentrations at 4–5 h. This fact caused a slow but prolonged reduction in blood glucose levels, which indicated the continuing pharmacological activity of the absorbed insulin. Compared with the group given the capsule without SBC, the group given the capsule with SBC revealed a faster and greater absorption of insulin, resulting in a more substantial hypoglycemic effect. For the cases without and with SBC, Table 1 shows that the maximum plasma concentrations were 34.0 ± 6.4 and 68.4 ± 6.8 μIU/mL, the AUC (0–10 h) values were 123.8 ± 28.4 and 249.2 ± 34.1 μIU h/mL, and the corresponding relative BA_R values were 10.8 ± 3.1 and 21.7 ± 1.7% ($P < 0.05$), respectively.

Conversely, administration of the capsules containing protease inhibitors/absorption enhancers (DTPA and SDS) produced a slow but prolonged reduction in blood glucose levels, which indicated the continuing pharmacological activity of the absorbed insulin. Compared with the group given the capsule without SBC, the group given the capsule with SBC revealed a faster and greater absorption of insulin, resulting in a more substantial hypoglycemic effect. For the cases without and with SBC, Table 1 shows that the AUC (0–10 h) values were 123.8 ± 28.4 and 249.2 ± 34.1 μIU h/mL, and the corresponding relative BA_R values were 10.8 ± 3.1 and 21.7 ± 1.7% ($P < 0.05$), respectively. These results suggest that oral administration of insulin using our bubble carriers may reduce the risk of hyperinsulinemia which has been commonly observed in patients receiving insulin subcutaneously.

4. Conclusion

The above results reveal that the bubble carrier system developed in the study considerably enhances the dispersion of insulin molecules released from an enteric-coated capsule transiting the intestinal tract. Since the transported DTPA and SDS serve as both protease inhibitors and absorption enhancers, they improve the oral bioavailability of insulin and induce hypoglycemic effects. In addition to oral administration of insulin, the proposed bubble carrier system has potential applications as a platform for oral administration of other therapeutic proteins.

Conflict of interest

None.

Acknowledgments

The authors would like to thank the Ministry of Science and Technology, Taiwan, for financially supporting this research under Contract No. NSC 103-2120-M-007-009-CC1. The molecular-imaging study was partially supported by grants CMRP391513 and CMRPG3A0512 from Chang Gung Memorial Hospital, Linkou, Taiwan. The NSRRC is gratefully acknowledged for providing technical support for the synchrotron X-ray scattering experiment.

Appendix A. Supplementary data

Supplementary data related to this article can be found at http://dx.doi.org/10.1016/j.biomaterials.2015.06.035.

References

[1] A. des Rieux, V. Fievez, M. Garinot, Y.J. Schneider, V. Préat, Nanoparticles as potential oral delivery systems of proteins and vaccines: a mechanistic approach, J. Control Release 116 (2006) 1–27.

[2] F.Y. Su, K.J. Lin, K. Sonaje, S.P. Wey, T.C. Yen, Y.C. Ho, et al., Protease inhibition and absorption enhancement by functional nanoparticles for effective oral insulin delivery, Biomaterials 33 (2012) 2801–2811.

[3] C.W. Pouton, Lipid formulations for oral administration of drugs: non-emulsifying, self-emulsifying and 'self-microemulsifying' drug delivery systems, Eur. J. Pharm. Sci. 11 (2000) S93–S98.

[4] J.F. Harper, G. Brooker, Femtomole sensitive radioimmunoassay for cyclic AMP and cyclic GMP after 2'0 acetylation by acetic anhydride in aqueous solution, J. Cycl. Nucleotide Res. 1 (1975) 207–218.

[5] C.J. Ke, T.Y. Su, H.L. Chen, H.L. Liu, W.L. Chiang, P.C. Chu, et al., Smart multifunctional hollow microspheres for the quick release of drugs in intracellular lysosomal compartments, Angew. Chem. Int. Ed. 123 (2011) 8236–8239.

[6] S.M. Deane, F.T. Robb, D.R. Woods, Production and activation of an SDS-resistant alkaline serine exoprotease of vibrio alginolyticus, J. Gen. Microbiol. 133 (1987) 391–398.

[7] J.C. Riemersma, Osmium tetroxide fixation of lipids: nature of the reaction products, J. Histochem. Cytochem. 11 (1963) 436–442.

[8] S.F. Peng, M.J. Yang, C.J. Su, H.L. Chen, P.W. Lee, M.C. Wei, et al., Effects of incorporation of poly(γ-glutamic acid) in chitosan/DNA complex nanoparticles on cellular uptake and transfection efficiency, Biomaterials 30 (2009) 1797–1808.

[9] M.K. Marschutz, P. Caliceti, A. Bernkop-Schnurch, Design and *in vivo* evaluation of an oral delivery system for insulin, Pharm. Res. 17 (2000) 1468–1474.

[10] B. Jang, S. Park, S.H. Kang, J.K. Kim, S.K. Kim, I.H. Kim, et al., Gold nanorods for target selective SPECT/CT imaging and photothermal therapy *in vivo*, Quant. Imaging Med. Surg. 2 (2012) 1–11.

[11] E.Y. Chuang, K.J. Lin, F.Y. Su, F.L. Mi, B. Maiti, C.T. Chen, et al., Noninvasive imaging oral absorption of insulin delivered by nanoparticles and its stimulated glucose utilization in controlling postprandial hyperglycemia during OGTT in diabetic rats, J. Control Release 172 (2013) 513–522.

[12] E.Y. Chuang, K.J. Lin, F.Y. Su, H.L. Chen, B. Maiti, Y.C. Ho, et al., Calcium depletion-mediated protease inhibition and apical-junctional-complex disassembly via an EGTA-conjugated carrier for oral insulin delivery, J. Control Release 169 (2013) 296–305.

[13] M.Z.I. Khan, Ž. Prebeg, N. Kurjaković, A pH-dependent colon targeted oral drug delivery system using methacrylic acid copolymers: I. manipulation of drug release using Eudragit® L100-55 and Eudragit® S100 combinations, J. Control Release 58 (1999) 215–222.

[14] F. De Jaeghere, E. Allémann, F. Kubel, B. Galli, R. Cozens, E. Doelker, et al., Oral bioavailability of a poorly water soluble HIV-1 protease inhibitor incorporated into pH-sensitive particles: effect of the particle size and nutritional state, J. Control Release 68 (2000) 291–298.

[15] D.F. Evans, G. Pye, R. Bramley, A.G. Clark, T.J. Dyson, J.D. Hardcastle, Measurement of gastrointestinal pH profiles in normal ambulant human subjects, Gut 29 (1988) 1035–1041.

[16] K. Sonaje, Y.J. Chen, H.L. Chen, S.P. Wey, J.H. Juang, H.N. Nguyen, et al., Enteric-coated capsules filled with freeze-dried chitosan/poly(γ-glutamic acid) nanoparticles for oral insulin delivery, Biomaterials 31 (2010) 3384–3394.

[17] C.I.K. Diop, H.L. Li, B.J. Xie, J. Shi, Effects of acetic acid/acetic anhydride ratios on the properties of corn starch acetates, Food Chem. 126 (2011) 1662–1669.

[18] K.J. Chen, E.Y. Chuang, S.P. Wey, K.J. Lin, F. Cheng, C.C. Lin, et al., Hyperthermia-mediated local drug delivery by a bubble-generating liposomal system for tumor-specific chemotherapy, ACS Nano. 8 (2014) 5105–5115.

[19] G.M. Flores-Fernández, R.J. Solá, K. Griebenow, The relation between moisture-induced aggregation and structural changes in lyophilized insulin, J. Pharm. Pharmacol. 61 (2009) 1555–1561.

[20] D. Knebel, M. Sieber, R. Reichelt, H.J. Galla, M. Amrein, Scanning force microscopy at the air-water interface of an air bubble coated with pulmonary surfactant, Biophys. J. 82 (2002) 474–480.

[21] F. Araújo, P. Fonte, H.A. Santos, B. Sarmento, Oral delivery of glucagon-like peptide-1 and analogs: alternatives for diabetes control? J. Diabetes Sci. Technol. 6 (2012) 1486–1497.

[22] E. Roger, F. Lagarce, E. Garcion, J.P. Benoit, Lipid nanocarriers improve paclitaxel transport throughout human intestinal epithelial cells by using vesicle-mediated transcytosis, J. Control Release 140 (2009) 174–181.

[23] L.W. Hsu, Y.C. Ho, E.Y. Chuang, C.T. Chen, J.H. Juang, F.Y. Su, et al., Effects of pH on molecular mechanisms of chitosan–integrin interactions and resulting tight-junction disruptions, Biomaterials 34 (2013) 784–793.

[24] R.C. Brown, T.P. Davis, Calcium modulation of adherens and tight junction function: a potential mechanism for blood-brain barrier disruption after stroke, Stroke 33 (2002) 1706–1711.

[25] A.I. Ivanov, A. Nusrat, C.A. Parkos, Endocytosis of epithelial apical junctional proteins by a clathrin-mediated pathway into a unique storage compartment, Mol. Biol. Cell 15 (2004) 176–188.

[26] M. Thanou, J.C. Verhoef, H.E. Junginger, Oral drug absorption enhancement by chitosan and its derivatives, Adv. Drug Deliv. Rev. 52 (2001) 117–126.

[27] P.D. Ward, T.K. Tippin, D.R. Thakker, Enhancing paracellular permeability by modulating epithelial tight junctions, Pharm. Sci. Technol. Today 3 (2000) 346–358.

[28] S. Trier, L. Linderoth, S. Bjerregaard, T.L. Andresen, U.L. Rahbek, Acylation of glucagon-like peptide–2: interaction with lipid membranes and *in vitro* intestinal permeability, PLoS One 9 (2014) e109939.

[29] I. Ihse, P. Lilja, I. Lundquist, Trypsin as a regulator of pancreatic secretion in the rat, Scand. J. Gastroenterol. 14 (1979) 873–880.

[30] T. Yamagata, M. Morishita, N.J. Kavimandan, K. Nakamura, Y. Fukuoka, K. Takayama, et al., Characterization of insulin protection properties of complexation hydrogels in gastric and intestinal enzyme fluids, J. Control Release 112 (2006) 343–349.

[31] H. Mu, S.M. Zhou, Y. Xia, H. Zou, F. Meng, Y.B. Yan, Inactivation and unfolding of the hyperthermophilic inorganic pyrophosphatase from thermus thermophilus by sodium dodecyl sulfate, Int. J. Mol. Sci. 10 (2009) 2849–2859.

[32] C.J.H. Porter, N.L. Trevaskis, W.N. Charman, Lipids and lipid-based formulations: optimizing the oral delivery of lipophilic drugs, Nat. Rev. Drug Discov. 6 (2007) 231–248.